Title

Anisotropic E × B shearing rate in a magnetic island

Journal

Physics of Plasmas, 28(2)

ISSN

1070-664X

Authors

Hahm, TS
Kim, YJ
Diamond, PH
et al.

Publication Date

2021-02-01

DOI

10.1063/5.0036583

Peer reviewed

AIP/123-QED

Anisotropic ExB shearing rate in a magnetic island

T. S. Hahm,[1, a)] Y. J. Kim,[1] P. H. Diamond,[2] and G. J. Choi[3]

[1)]*Department of Nuclear Engineering, Seoul National University, Seoul 08826, Republic of Korea*

[2)]*Center for Astrophysics and Space Sciences (CASS), University of California, San Diego, La Jolla, California 92093, USA.*

[3)]*Department of Physics and Astronomy, University of California, Irvine, California 92697, USA.*

(Dated: 7 January 2021)

We derive the ExB shearing rate associated with vortex flow inside a macroscopic magnetic island (MI) in axisymmetric toroidal geometry. Due to the elongation of the MI and incompressibility of the ExB flow, the shearing rate near X-points is much lower than that near the mid-plane (x-axis of the local Cartesian coordinate) of the MI on the same flux surface. Furthermore, the rate formally vanishes at the X-points where the local poloidal magnetic field associated with the MI stagnates. This calculation of ExB shearing profile and, in particular minimal ExB shear near the X-points is consistent with the recent experimental finding that turbulence tends to spread into an MI through regions around the X-points[K. Ida et al., Phys. Rev. Lett. 120, 245001 (2018)], and can contribute to more thorough quantitative interpretation of the results from experiments and simulations.

[a)]Electronic mail: tshahm@snu.ac.kr

I. INTRODUCTION

Despite considerable progress made in experiment, theory, and simulation in achieving high performance of magnetically confined plasmas, several challenges remain in understanding, predicting and controlling turbulent transport. One outstanding problem involves multi-scale interaction between macroscopic structures and microturbulence for which a variety of nondiffusive phenomena plays a crucial role as recently reviewed.[1]

Among them, the MI-turbulence interaction is a topic of high interest currently and has been reviewed recently with an emphasis on experiment[2] and simulation[3] respectively. A large MI commonly degrades confinement and is considered to be a major concern for a successful operation of ITER.[4] On the other hand, its existence has been sometimes attributed as a contributing factor to internal transport barrier formation near low order rational surface.[2] Therefore, turbulence behavior around an MI is a fusion-relevant and scientifically stimulating subject which requires further thorough understanding.

Turbulence can exist inside an MI where the pressure gradient is not sufficiently sharp for a linear instability. This can happen due to turbulence spreading[5–7] from outside the separatrix where the gradients are strong enough. Meanwhile turbulence driven ExB zonal flow shear can regulate turbulence[8] and it should work inside an MI as well. Indeed, nonlinear gyrokinetic simulations demonstrated that strong enough ExB flow shear quantified by the shearing rate in Ref. 9 can not only reduce turbulence locally,[10] but is also effective in blocking turbulence spreading.[11]

Recent experimental results indicate that turbulence can access the interior of a magnetic island or can be excluded, resulting in high accessibility (worse confinement) or low accessibility (good confinement) states.[12] Results also indicate that the X-point region acts as a 'valve', which, when open, allows turbulence to spread into the island and, when closed, blocks such penetration.[13] Clearly, the local physics of ExB shearing near the X-point is relevant to the 'valve' mechanism and to whether or not turbulence can penetrate the island. To this end, in this paper we calculate the ExB shearing rate in an MI. In particular, we determine the anisotropy of the shearing rate, and show that shearing is weakest at the X-point, i.e. the location of the 'valve'. This is at least consistent with the experimental observation that turbulence accesses the island interior via the X-point. We assume that the ExB flow inside a macroscopic MI has a vortex structure and that its associated electrostatic potential Φ is a function of the MI-distorted flux.

The principal results of this paper are:

(i) We have derived the ExB shearing rate inside the MI, using two-point decorrelation theory in the presence of the ExB flow,[9,14,15]

$$\omega_{ExB} = \left(\frac{k_y W}{2}\sqrt{1-\left(\frac{\rho}{W}\right)^2 \sin^2\chi}\right)\left(\frac{\Delta\rho}{\rho\Delta\chi}\right)\frac{\partial^2}{\partial\psi_\rho^2}\Phi(\psi_\rho).$$

Here, $k_y = \frac{m}{r_0}$ is the wave number of the MI with the poloidal mode number m. W is the MI half radial width. (ρ,χ) is a polar coordinate in the MI. $\Delta\rho$ and $\rho\Delta\chi$ are the turbulence eddy size in each direction. $\psi_\rho = \frac{1}{2}B\rho^2$ is the flux function inside the MI. The first factor comes from the MI-geometry and the coordinates used. The second factor is the turbulence eddy aspect ratio in the polar coordinate inside the MI. Both reflect the effects of MI-elongation and the existence of X-points where the magnetic field orthogonal to the toroidal direction vanishes.

(ii) The shearing rate exhibits a highly anisotropic structure. Its value is much lower by a factor $\sim (k_y W)^2$ at the y-axis, near the X-point, as compared to that at the x-axis (the mid-plane of the MI) on the same flux surface. This is due to the incompressibility of the ExB flow in a strongly magnetized plasma and the MI-elongation.

(iii) In addition, the shearing rate vanishes at the X-points $(\rho,\chi) = (W,\pm\frac{\pi}{2})$, as

$$\propto \sqrt{1-\left(\frac{\rho}{W}\right)^2 \sin^2\chi}.$$

This is related to the fact that B_χ vanishes at the X-points. From this, we conclude that turbulence may spread easily from outside to inside of the MI through the X-point region. This is consistent with the recent experimental result which demonstrates that turbulence tends to spread from the X-point to the O-point.[16]

The remainder of this paper is organized as follows. The MI-geometry is described and the polar coordinate inside is introduced in Sec. II. In Sec. III, the two point decorrelation calculation is performed for one field flute-like fluctuations. Then, the ExB shearing rate inside the MI is derived. In Sec. IV, the spatial structure of the ExB shearing rate is described in detail. In particular, the anisotropy of the rate and its behavior near X-points are discussed. Finally, several remaining issues related to this research are described in Sec. V.

II. THEORETICAL MODEL

We consider an axisymmetric, high aspect ratio, circular geometry for the zero-th order equilibrium magnetic field,

$$\vec{B}_0 = I\nabla\zeta + \nabla\zeta \times \nabla\psi_0, \tag{1}$$

where ζ is the toroidal angle, ψ_0 is the unperturbed poloidal flux which is related to the radial coordinate by $d\psi_0 = RB_\theta dr$. The first term on the right hand side (RHS) is the toroidal magnetic field with $B_\phi = I/R$, the second term is the poloidal magnetic field $\vec{B}_\theta = \frac{1}{R}\frac{\partial\psi_0}{\partial r}\hat{e}_\theta$.

We assume the equilibrium is distorted by a single helicity static MI located at the rational surface r_s, where $q(r_s) = \frac{m}{n}$ "n" and "m" are the toroidal and poloidal mode numbers respectively. We consider a macroscopic MI with $m = nq(r_s) = O(1)$, which can be either spontaneously generated[17] or forced externally.[18] Its associated poloidal flux is given by

$$\delta\psi = \delta\bar{\psi}\cos\xi, \tag{2}$$

where $\xi = m\theta - n\zeta = m\left(\theta - \frac{\zeta}{q(r_s)}\right)$, $\theta - \frac{\zeta}{q(r_s)}$ is the helical angle along $\vec{B}_0$. We use the constant-ψ approximation[17] for $\delta\psi$ around r_s which is applicable to MIs except for $(m,n) = (1,1)$ mode. Our model equilibrium distorted by an MI is then given by

$$\vec{B} = I\nabla\zeta + \nabla\zeta \times \nabla(\psi_0 + \delta\psi). \tag{3}$$

We assume $|\vec{B}|$ is not affected by the presence of an MI. For explicit analyses around an MI, it is convenient to work with a flux function Ω which demonstrates the MI structure clearly,

$$\Omega = \frac{2(r-r_s)^2}{W^2} - \cos\xi. \tag{4}$$

The half width of an MI is given by

$$W = 2\left[\frac{\delta B_r}{k_\theta B/L_s}\right]^{1/2} = 2\left[\frac{q}{\hat{s}}\frac{\delta\bar{\psi}}{B}\right]^{1/2}, \tag{5}$$

where $L_s = qR_0/\hat{s}$ and $\hat{s}$ is the magnetic shear.

Here, the equilibrium $B_\theta(r_s)$ at the rational surface is subtracted from $B_\theta(r)$ and it appears only in terms of its radial derivative in the standard sheared slab model,[19]

$$\vec{B}_y = \hat{y}\left(\frac{\partial B_y}{\partial x}\right)x = -\hat{y}\frac{B}{L_s}x. \tag{6}$$

This leads to Eqs. (4) and (5) with widely used notations.[20–22] For a clear illustration of the MI geometry, we introduce a "polar" coordinate defined by

$$\rho\cos\chi = x, \tag{7a}$$

$$\rho\sin\chi = W\sin\left(\frac{k_y}{2}y\right), \tag{7b}$$

and

$$\rho^2 = \left(\frac{\Omega+1}{2}\right)W^2 = x^2 + W^2\sin^2\left(\frac{k_y}{2}y\right). \tag{8}$$

Here (x,y) is the Cartesian coordinate with $\xi = k_y y$. We note that this geometry is also familiar from a simple model for double-null diverted tokamak equilibrium.[23] This similarity has been utilized in both ways.[23,24] This is shown in Fig. 1. Inside the MI, it can be shown that

$$\begin{aligned} B_\rho &= 0, \\ B_\chi &= \frac{\delta\overline{\psi}}{R}|\nabla\Omega| \\ &= B_\theta(r_s)\left(\frac{W}{L_s}\right)\left[\left(\frac{\rho}{W}\right)^2\cos^2\chi + \left(\frac{k_y\rho}{2}\right)^2\sin^2\chi\left(1-\left(\frac{\rho}{W}\right)^2\sin^2\chi\right)\right]^{1/2} \end{aligned}$$

At the X-points $(\rho,\chi) = (W, \pm\frac{\pi}{2})$, B_χ vanishes. So $\vec{B}_\chi$ lingers around these stagnation points. A strong magnetic field B in ζ direction orthogonal to (ρ,χ) plane is taken to be a constant because its spatial variation is small within the MI.

Finally, we assume that the electrostatic potential Φ is a function of ρ only. This will lead to a vortex structure of the ExB flows along $\vec{B}_\chi$ inside an MI. There is evidence from experiments[25,26] and simulations[27–32] that an ExB vortex rotating around the O-point can exist inside an MI. A longer list of references can be found from recent reviews.[2,3] For a $\Phi(\psi_\rho)$, the ExB flow in our coordinate can be written as

$$\vec{u}_{ExB} = -\frac{\nabla\Phi\times\vec{B}}{B^2} = \frac{1}{B}\left(\frac{\partial\Phi}{\partial\rho}\right)\hat{b}\times\nabla\rho. \tag{9}$$

Considering flute-like perturbations $\delta H(\rho,\chi)$, the ExB convection term becomes

$$\begin{aligned} \vec{u}_{ExB}\cdot\nabla\delta H &= \frac{1}{B}\left(\frac{\partial\Phi}{\partial\rho}\right)\hat{b}\times\nabla\rho\cdot\left[\nabla\chi\frac{\partial\delta H}{\partial\chi} + \nabla\rho\frac{\partial\delta H}{\partial\rho}\right] \\ &= \frac{1}{B}\left(\frac{\partial\Phi}{\partial\rho}\right)(\hat{b}\cdot\nabla\rho\times\nabla\chi)\frac{\partial}{\partial\chi}\delta H. \end{aligned} \tag{10}$$

Since the inverse of Jacobian of the coordinate $(\hat{b}\cdot\nabla\rho\times\nabla\chi) = \frac{k_y W}{2\rho}\sqrt{1-\left(\frac{\rho}{W}\right)^2\sin^2\chi}$ contains the MI-elongation factor $k_y W$ and asymptotes to zero at the X-points, it is convenient to work with

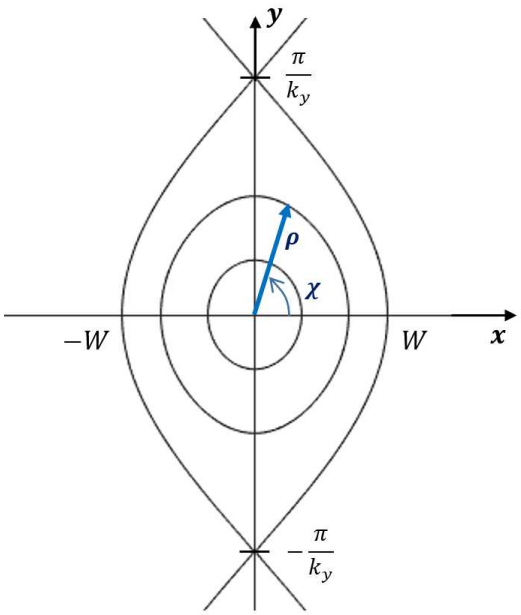

FIG. 1. A simple MI model equilibrium and associated polar coordinate inside an MI. X-points are located at $(\rho,\chi)=(W,\pm\frac{\pi}{2})$ and $(x,y)=(0,\pm\frac{\pi}{k_y})$

another angle χ_0 satisfying

$$\left(\frac{k_y W}{2}\right)\sqrt{1-\left(\frac{\rho}{W}\right)^2\sin^2\chi}\frac{\partial}{\partial\chi}=\frac{\partial}{\partial\chi_0}. \tag{11}$$

Then, Eq. (10) becomes

$$\begin{aligned}\vec{u}_{ExB}\cdot\nabla\delta H&=\frac{1}{B}\left(\frac{\partial\Phi}{\partial\rho}\right)[\hat{b}\cdot\nabla\rho\times\nabla\chi_0]\frac{\partial}{\partial\chi_0}\delta H\\&=\left(\frac{\partial\Phi}{\partial\psi_\rho}\right)\frac{\partial}{\partial\chi_0}\delta H(\chi_0,\rho),\end{aligned} \tag{12}$$

where $\psi_\rho=\frac{1}{2}B\rho^2$.

III. TWO-POINT DECORRELATION ANALYSES

Following the previous work,[9,14,15,33,34] we can construct the two-point correlation evolution equation for a one-field fluid quantity δH (for instance, density fluctuation δn or electron temper-

ature fluctuation δT_e). We consider flute-like fluctuations and work in a two-dimension (ψ_ρ, χ_0). Following the standard procedure of symmetrization with respect to the two points and ensemble averaging,[35] we obtain

$$\left[\frac{\partial}{\partial t} - \psi_- \left(\frac{\partial^2}{\partial \psi_\rho^2}\Phi\right)\frac{\partial}{\partial \chi_-} - D_-^{\rm eff}\frac{\partial^2}{\partial \chi_-^2}\right]\langle \delta H(1)\delta H(2)\rangle = S_2. \tag{13}$$

Here, $\dfrac{\partial^2}{\partial \psi_\rho^2}\Phi$ corresponds to the radial shear of the vortex rotation angular frequency in the χ_0-direction. Subscripts "-" refer to the difference between two points $(\psi_{\rho 1}, \chi_{01})$ and $(\psi_{\rho 2}, \chi_{02})$. S_2 is the source term for the two-point correlation function and the ExB nonlinearity is approximated as a turbulent diffusion along the χ_0-direction. We use the following asymptotic form of the relative diffusion $D_-^{\rm eff}$ at a small separation,

$$D_-^{\rm eff} = 2D^{\rm eff}\left[\left(\frac{\psi_-}{\Delta\psi_{\rho 0}}\right)^2 + \left(\frac{\chi_-}{\Delta\chi_0}\right)^2\right], \tag{14}$$

where $D^{\rm eff} = \Delta\omega_T \Delta\chi_0^2/4$, $\Delta\omega_T$ is the turbulence decorrelation rate $\sim$ [eddy life time]$^{-1}$.

By taking various moments of the LHS of Eq. (13), we can investigate the decorrelation due to the coupling between the flow shear and turbulent diffusion. Using the two point Green's function for the LHS of Eq. (13), we can define various moments according to,

$$\langle A(\psi_-, \chi_-)\rangle \equiv \int d\psi'_- d\chi'_- G(\psi_-, \chi_- | \psi'_-, \chi'_-) A(\psi'_-, \chi'_-).$$

These satisfy the following equations,

$$\partial_t \langle \psi_-^2\rangle = 0, \tag{15a}$$

$$\partial_t \langle \chi_-^2\rangle = 4D^{\rm eff}\left[\frac{\langle \psi_-^2\rangle}{\Delta\psi_{\rho 0}^2} + \frac{\langle \chi_-^2\rangle}{\Delta\chi_0^2}\right] - 2\left[\frac{\partial^2}{\partial\psi_\rho^2}\Phi(\psi_\rho)\right]\langle \psi_-\chi_-\rangle \tag{15b}$$

and

$$\partial_t \langle \psi_-\chi_-\rangle = -\left[\frac{\partial^2}{\partial\psi_\rho^2}\Phi(\psi_\rho)\right]\langle \psi_-^2\rangle. \tag{15c}$$

Integration of Eqs. (15a)-(15c) yields a solution which has the following long term asymptotic form for $\Delta\omega_T t > 1$:

$$\frac{\langle \chi_-^2\rangle(t)}{\Delta\chi_0^2} = \left[\frac{\psi_-^2}{\Delta\psi_{\rho 0}^2}\left\{1 + \left(\frac{\Delta\psi_{\rho 0}}{\Delta\omega_T\Delta\chi_0}\right)^2\left(\frac{\partial^2}{\partial\psi_\rho^2}\Phi\right)^2\right\} + \frac{1}{\Delta\chi_0^2}\left\{\chi_- - \frac{1}{\Delta\omega_T}\left(\frac{\partial^2}{\partial\psi_\rho^2}\Phi\right)\psi_-\right\}^2\right] e^{\Delta\omega_T t}. \tag{16}$$

From Eq. (16), we can define the eddy life time as a function of the initial separation between two nearby points characterized by χ_- and ψ_-.

$$\tau_{\text{eddy}} = \Delta\omega_T^{-1} \ln([\cdots]^{-1}), \tag{17}$$

where $[\cdots]$ is the expression multiplying $e^{\Delta\omega_T t}$ on the RHS of Eq. (16). Eq. (14) implies $[\cdots] < 1$. The radial correlation length $\Delta\rho \equiv \dfrac{\Delta\psi_\rho}{\rho B}$ is reduced by the ExB flow shear relative to its value $\Delta\rho_0 = \dfrac{\Delta\psi_{\rho 0}}{\rho B}$ determined by ambient turbulence alone:

$$\left(\frac{\Delta\psi_{\rho 0}}{\Delta\psi_\rho}\right)^2 = 1 + \frac{\omega_{ExB}^2}{\Delta\omega_T^2}. \tag{18}$$

Therefore, we expect that fluctuation suppression occurs when the decorrelation rate of the ambient turbulence $\Delta\omega_T$ is exceeded by the ExB shearing rate ω_{ExB} given by

$$\omega_{ExB}^2 = \left(\frac{\Delta\psi_{\rho 0}}{\Delta\chi_0}\right)^2 \left|\frac{\partial^2}{\partial\psi_{\rho 0}^2}\Phi(\psi_{\rho 0})\right|^2. \tag{19}$$

IV. SPATIAL STRUCTURE OF THE EXB SHEARING RATE

The following expression from Eq. (19) is formally identical to that in Ref. 9, but the definitions of ψ_ρ and χ_0 are quite different,

$$\omega_{ExB} = \left(\frac{\Delta\psi_\rho}{\Delta\chi_0}\right)\left|\frac{\partial^2}{\partial\psi_\rho^2}\Phi(\psi_\rho)\right|. \tag{20}$$

The last factor is constant on the same flux surface defined by $\psi_\rho = \frac{1}{2}B\rho^2 = \text{constant}$. However, $\dfrac{\Delta\psi_\rho}{\Delta\chi_0}$ is proportional to the eddy aspect ratio and can vary in χ and ρ. Using Eq. (11),

$$\frac{\Delta\psi_\rho}{\Delta\chi_0} = \frac{k_y W}{2}\sqrt{1 - \left(\frac{\rho}{W}\right)^2 \sin^2\chi}\left(\frac{\Delta\rho}{\rho\Delta\chi}\right)B\rho^2. \tag{21}$$

$\dfrac{\Delta\rho}{\rho\Delta\chi}$ is the eddy aspect ratio in (ρ,χ) coordinate. Due to the elongated MI-geometry ($\dfrac{1}{k_y} \gg W$ for most low-m islands), ρ-contours are sparsely distributed along y-axis. Furthermore, the effect associated with the $\vec{B}_\chi$ stagnation near X-points can be significant.

For $\chi = 0$, along the mid-plane (x-axis) of an MI, we can show $\dfrac{\Delta\rho}{\rho\Delta\chi} \simeq \left(\dfrac{2}{k_y W}\right)\dfrac{\Delta x}{\Delta y}$ using Eqs. (7a), (7b) and (8). Here, Δx and Δy are the eddy size along the Cartesian coordinate. A factor

$\frac{2}{k_y W}$, however, is cancelled by the first factor of $\frac{\Delta\psi_0}{\Delta\chi_0}$ in Eq. (21). Therefore, along $\chi = 0$ (x-axis),

$$\omega_{ExB} \simeq \left(\frac{\Delta x}{\Delta y}\right) B\rho^2 \left(\frac{\partial^2}{\partial \psi_\rho^2}\Phi\right). \tag{22}$$

$\frac{\Delta x}{\Delta y}$ is the expected eddy shape aspect ratio showing that the radially elongated eddys in tokamak $\left(\frac{\Delta x}{\Delta y} > 1\right)$ are easier to shear-decorrelate. The last factor is a flux function. Eq. (22) is an expression one would have expected from a simple heuristic consideration. For instance, the local expression $\frac{\Delta x}{\Delta y}\frac{1}{B}\frac{\partial}{\partial x}u_y$ recovers Eq. (22).

On the other hand, for $\chi = \frac{\pi}{2}$ along the rational surface (y-axis) of the MI, from the O-point toward the X-points at $(\rho,\chi) = (W, \pm\frac{\pi}{2})$, one can show that

$$\frac{\Delta\rho}{\rho\Delta\chi} \simeq \left(\frac{k_y W}{2}\right)\frac{\Delta y}{\Delta x}.$$

Then, the shearing rate in Eq. (20) becomes

$$\omega_{ExB} \simeq \left(\frac{k_y W}{2}\right)^2 \sqrt{1-\left(\frac{\rho}{W}\right)^2}\frac{\Delta y}{\Delta x}\left(B\rho^2\frac{\partial^2\Phi}{\partial\psi_\rho^2}\right). \tag{23}$$

Here, the eddy aspect ratio factor is flipped to $\frac{\Delta y}{\Delta x}$ as it should because the local ExB flow from the vortex is now in x direction. So near the rational surface, it is harder to shear-suppress a radially elongated eddy in tokamak with $\frac{\Delta y}{\Delta x} < 1$. We note that some nonlinear simulations show appearance of radially elongated eddys around an MI.[29,30,36]

Most importantly, the first geometric factor $\frac{k_y W}{2}\sqrt{1-(\frac{\rho}{W})^2}$ exhibits a significant reduction of the shearing rate, in particular as one approaches the X-points $\rho \to W$. This is related to $\vec{B}_x$ lingering around that stagnation point.

Since the ExB vortex flow for a strong equilibrium B is incompressible and the MI is highly elongated along y direction, u_x around the y-axis becomes much slower than u_y around the x-axis at the same flux surface $\psi_\rho(\rho)$. From the incompressibility constraint,

$$u_x\left(\chi = \frac{\pi}{2}\right) \simeq (k_y W)u_y(\chi = 0) = \left(\frac{mW}{r}\right)u_y(\chi = 0).$$

Therefore, we can expect the ExB shear near $\chi = \pi/2$ can be reduced by a factor $O(\frac{mW}{r})$ compared to that near $\chi = 0$. In addition, the shearing rate vanishes at the X-points where B_χ also vanishes.

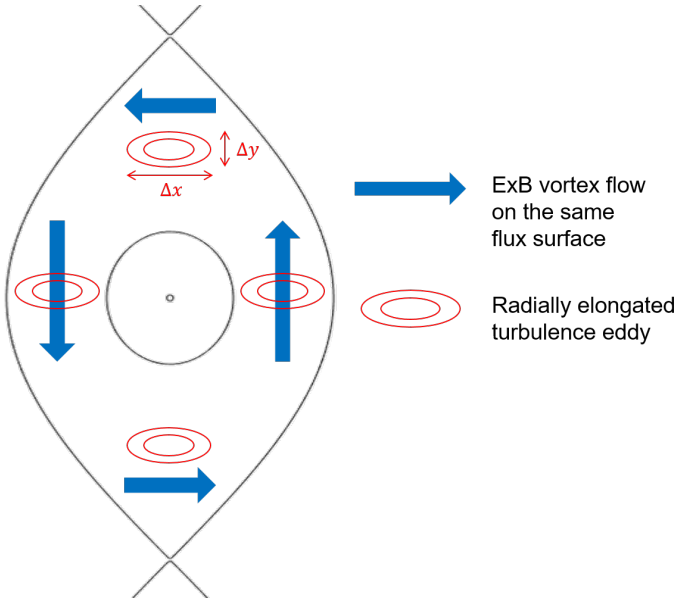

FIG. 2. Incompressible vortex flow and radially elongated eddy.

Turbulence spreading from outside of an MI into the interior has been widely observed from simulations,[27,28,37,38] for instance. However, recall that turbulence spreading can be blocked if the shearing rate is high enough as demonstrated from nonlinear gyrokinetic simulations.[11] The reduction of the shearing rate near the X-point may be related to the observations from recent experiment[16,39] that turbulence spreading from outside of an MI into the interior occurs mainly through the X-point region.

Figure 2 illustrates that the ExB vortex flow is weaker near X-points compared to that near mid-plane due to incompressibility. Radially elongated (in tokamak coordinate "r") eddy is shown in red circles to show easier shearing at the mid-plane. The shearing rate is proportional to $\frac{\Delta x}{\Delta y}\frac{\partial u_y}{\partial x}$ near mid-plane and to $\frac{\Delta y}{\Delta x}\frac{\partial u_x}{\partial y}$ near X-points.

V. DISCUSSION

In this section, we discuss several key issues which have not been considered in this paper. First, while the vortex flow has been widely observed in experiments[2,25,26] and nonlinear

simulations,[3,27–30] its generation mechanism has not been identified. A few possibilities include the following.

i) Turbulence which exists inside of an MI due to spreading from outside can generate a vortex via nonlinear interaction. This should be similar to the zonal flow generation through Reynolds stress in open field lines.[8,40] In particular, the small scale coherent vortex (SSCV)[41] may merge into a vortex of the MI-size.

ii) ExB flows (either externally driven or turbulence-generated) just outside the separatrix can act as a boundary condition affecting the vortex flow inside the MI. Some experimental results indicate a possibility of this mechanism.[42]

Second, this work is based on a simple model and can be extended in the future addressing the following issues.

(i) Some simulations report that the vortex flow evolves in time with a scale as fast as the geodesic acoustic mode (GAM) period.[27,30] While it requires further research to determine if it also happens in experiment, the time dependence of the ExB flows can be included in the analysis following the method in Ref. 43. The low frequency part of the ExB flow shear with $\omega_{flow} < \Delta\omega_T$ is more effective in suppressing turbulence.[43] In addition, the GAM wave group propagation can play a role in turbulence spreading.[44]

(ii) The MI-geometry adopted for our analysis is a standard model widely used for research related to a finite size MI.[19–22] It uses a coordinate in which $B_\theta(r_s)$ at the vertical surface $r = r_s$ is zero and the effective poloidal $\vec{B}$ appears as $B_\theta(r)\hat{y} = -\dfrac{B}{L_s}(r - r_s)\hat{y}$. This is justified inside of an MI, but not applicable to the region away from it. Obviously the ExB flow shear outside the MI should also play some role in controlling turbulence spreading into the MI. The MI-geometric effect on this based on the shearing rate from Ref. 9 is also being pursued.[45]

(iii) As shown in the main text, the eddy shape influences the effectiveness of the ExB shearing considerably. In our analysis, we assumed that the eddy shape can be characterized by its dimension in two different directions only. However, there is another variable (i.e. the eddy tilting angle) which can influence the shearing effectiveness.[46] The inclusion of this effect is conceptually straightforward, but with a considerable amount of algebra. Experimental results on the MI-turbulence interaction[2,47–51] exhibit phenomena much richer than those addressed in this paper. In particular, recent findings[39] demonstrate intricate nonlocal effects

of turbulence on nonlinear evolution of an MI which clearly deserves further theoretical investigation.

(iv) Finally, it would be interesting to use the shearing rate from this work in a simple transport bifurcation model, with the aim of calculating the heat flux power threshold for the low accessibility state.[12] A likely road forward on this project is identified by considering the effects of ExB shearing (in the island geometry) on turbulence spreading and heat transport. Specifically, one might consider the coupled evolution of thermal transport and the flux of turbulence intensity in the presence of the island and the associated ExB shear. It is well known that ExB shear can reduce or suppress both types of turbulent transport. Moreover, here the determining factor in the suppression will be the shearing at near the X-point. That location is where the shear is weakest, and so turbulence is most likely to access the island. Once turbulence has penetrated the island, heat transport will increase. Hence, an analysis of the coupled heat and intensity transport equations, incorporating ExB shearing as represented by Eq. (20), seems like a promising approach to a model of the turbulence spreading transport bifurcation for the island. The model could be constructed using the island-specific shearing expression of Eq. (20). Feedback follows from the observation that stronger shear $\rightarrow$ weaker spreading $\rightarrow$ weaker transport inside the island $\rightarrow$ stronger shear, etc. A unique output of such an analysis would be a relation specifying the critical heat flux for an island ITB, as a function of island size. This analysis will be presented in a future publication.

ACKNOWLEDGMENTS

We acknowledge useful conversations with M.J. Choi, K. Ida, M. Jiang, W.X. Guo, A. Ishizawa, Y. Kishimoto, J.M. Kwon, Z. Lin, L. Wang, W.X. Wang, and E.S. Yoon. This work was supported by National R&D Program through the National Research Foundation of Korea(NRF) funded by the Ministry of Science, ICT and Future Planning (NRF-2019M1A7A1A02088355), U.S. DOE under Award No. DE-FG02-04ER 54738, and by U.S. Department of Energy, Office of Science, Office of Advanced Scientific Computing Research and Office of Fusion Energy Sciences, Scientific Discovery through Advanced Computing (SciDAC) program under Award Number DE-SC0018270 (SciDAC ISEP Center). In addition, T.S. Hahm, P.H. Diamond and G.J. Choi acknowledge useful interactions with participants during the Theorie-Fest held at Aix-en-Provence,

France in 2017 and 2019.

DATA AVAILABILITY

The data that support the findings of this study are available from the corresponding author upon reasonable request.

REFERENCES

[1]T. S. Hahm and P. H. Diamond, J. Korean Phys. Soc. 73, 747 (2018).

[2]K. Ida, Plasma Phys. Controlled Fusion 62, 014008 (2020).

[3]A. Ishizawa, Y. Kishimoto, and Y. Nakamura, Plasma Phys. Controlled Fusion 61, 054006 (2019).

[4]F. Turco, T. C. Luce, W. Solomon, G. Jackson, G. A. Navratil, and J. M. Hanson, Nucl. Fusion 58, 106043 (2018).

[5]X. Garbet, L. Laurent, A. Samain, and J. Chinardet, Nucl. Fusion 34, 963 (1994).

[6]T. S. Hahm, P. H. Diamond, Z. Lin, K. Itoh, and S.-I. Itoh, Plasma Phys. and Controlled Fusion 46, A323 (2004).

[7]O. D. Gurcan, P. H. Diamond, T. S. Hahm, and Z. Lin, Phys. Plasmas 12, 032303 (2005).

[8]P. H. Diamond, S.-I. Itoh, K. Itoh, and T. S. Hahm, Plasma Phys. Controlled Fusion 47, R35 (2005).

[9]T. S. Hahm and K. H. Burrell, Phys. Plasmas 2, 1648 (1995).

[10]Z. Lin, T. S. Hahm, W. Lee, W. M. Tang, and R. B. White, Science 281, 1835 (1998).

[11]W. X. Wang, T. S. Hahm, W. W. Lee, G. Rewoldt, J. Manickam, and W. M. Tang, Phys. Plasmas 14, 072306 (2007).

[12]K. Ida, T. Kobayashi, T. E. Evans, S. Inagaki, M. E. Austin, M. W. Shafer, S. Ohdachi, Y. Suzuki, S.-I. Itoh, and K. Itoh, Sci. Rep. 5, 16165 (2015).

[13]K. Ida, Advances in Physics: X 5, 1801354 (2020).

[14]H. Biglari, P. H. Diamond, and P. W. Terry, Phys. Fluids B 2, 1 (1990).

[15]T. S. Hahm, Phys. Plasmas 1, 2940 (1994).

[16]K. Ida, T. Kobayashi, M. Ono, T. E. Evans, G. R. McKee, and M. E. Austin, Phys. Rev. Lett. 120, 245001 (2018).

[17]H. P. Furth, J. Killeen, and M. N. Rosenbluth, Phys. Fluids 6, 459 (1963).

[18]T. S. Hahm and R. M. Kulsrud, Phys. Fluids 28, 2412 (1985).

[19]P. H. Rutherford, Phys. Fluids 16, 1903 (1973).

[20]J. W. Connor and H. R. Wilson, Phys. Plasmas 2, 4575 (1995).

[21]H. R. Wilson, J. W. Connor, R. J. Hastie, and C. C. Hegna, Phys. Plasmas 3, 248 (1996).

[22]F. L. Waelbroeck, Nucl. Fusion 49, 104025 (2009).

[23]T. S. Hahm and P. H. Diamond, Phys. Fluids 30, 133 (1987).

[24]A. Biancalani, L. Chen, F. Pegoraro, and F. Zonca, Phys. Rev. Lett. 105, 095002 (2010).

[25]K. Ida, N. Ohyabu, T. Morisaki, Y. Nagayama, S. Inagaki, K. Itoh, Y. Liang, K. Narihara, A. Yu. Kostrioukov, B. J. Peterson, K. Tanaka, T. Tokuzawa, K. Kawahata, H. Suzuki, A. Komori, and LHD Experimental Group, Phys. Rev. Lett. 88, 015002 (2001).

[26]T. Estrada, E. Ascasíbar, E. Blanco, A. Cappa, C. Hidalgo, K. Ida, A. López-Fraguas, and B. Ph van Milligen, Nucl. Fusion 56, 026011 (2016).

[27]W. A. Hornsby, A. G. Peeters, A. P. Snodin, F. J. Casson, Y. Camenen, G. Szepesi, M. Siccinio, and E. Poli, Phys. Plasmas 17, 092301 (2010).

[28]A. Bañón Navarro, L. Bardóczi, T. A. Carter, F. Jenko, and T. L. Rhodes, Plasma Phys. Controlled Fusion 59, 034004 (2017).

[29]J. M. Kwon, S. Ku, M. J. Choi, C. S. Chang, R. Hager, E. S. Yoon, H. H. Lee, and H. S. Kim, Phys. Plasmas 25, 052506 (2018).

[30]K. S. Fang and Z. Lin, Phys. Plasmas 26, 052510 (2019).

[31]K. Fang, J. Bao, and Z. Lin, Plasma Science and Technology 21, 115102 (2019).

[32]Z. Q. Hu, Z. X. Wang, L. Wei, J. Q. Li, Y. Kishimoto, X. D. Lin, and X. Gao, Nucl. Fusion 60, 056015 (2020).

[33]Y. Kosuga, S.-I. Itoh, P. H. Diamond, K. Itoh, and M. Lesur, Phys. Plasmas 21, 102303 (2014).

[34]G. J. Choi and T. S. Hahm, Phys. Plasmas 23, 072301 (2016).

[35]T. H. Dupree, Phys. Fluids 15, 334 (1972).

[36]A. Ishizawa and N. Nakajima, Nucl. Fusion 49, 055015 (2009).

[37]P. Hill, F. Hariri, and M. Ottaviani, Phys. Plasmas 22, 042308 (2015).

[38]E. Poli, A. Bottino, and A. G. Peeters, Nucl. Fusion 49, 075010 (2009).

[39]M. J. Choi, L. Bardóczi, J. M. Kwon, T. S. Hahm, H. K. Park, J. H. Kim, M. H. Woo, B. H. Park, G. S. Yun, E. S. Yoon, and G. McKee, to appear in Nat. Commun. (2021).

[40]M. N. Rosenbluth and F. L. Hinton, Phys. Rev. Lett. 80, 724 (1998).

[41]Z. B. Guo, T. S. Hahm, and P. H. Diamond, Phys. Plasmas 22, 122304 (2015).

[42]K. Ida, M. Yoshinuma, M. Yokoyama, S. Inagaki, N. Tamura, B. J. Peterson, T. Morisaki, S.

Masuzaki, A. Komori, Y. Nagayama, K. Tanaka, K. Narihara, K. Y. Watanabe, C. D. Beidler, and LHD experimental group, Nucl. Fusion 45, 391 (2005).

[43]T. S. Hahm, M. A. Beer, Z. Lin, G. W. Hammett, W. W. Lee, and W. M. Tang, Phys. Plasmas 6, 922 (1999).

[44]K. Miki and P. H. Diamond, Phys. Plasmas 17, 032309 (2010).

[45]W. Guo, M. Jiang and P. H. Diamond, Private communication (2019).

[46]G. J. Choi and T. S. Hahm, Nucl. Fusion 55, 093026 (2015).

[47]M. J. Choi, J. Kim, J.-M. Kwon, H. K. Park, Y. In, W. Lee, K. D. Lee, G. S. Yun, J. Lee, M. Kim, W.-H. Ko, J. H. Lee, Y. S. Park, Y.-S. Na, N. C. Luhmann Jr, and B. H. Park, Nucl. Fusion 57, 126058 (2017).

[48]L. Bardóczi, T. L. Rhodes, A. Bañón Navarro, C. Sung, T. A. Carter, R. J. La Haye, G. R. McKee, C. C. Petty, C. Chrystal, and F. Jenko, Phys. Plasmas 24, 056106 (2017).

[49]M. Jiang, W. L. Zhong, Y. Xu, Z. B. Shi, W. Chen, X. Q. Ji, X. T. Ding, Z. C. Yang, P. W. Shi, A. S. Liang, J. Wen, J. Q. Li, Y. Zhou, Y. G. Li, D. L. Yu, Y. Liu, Q. W. Yang, and the HL-2A Team, Nucl. Fusion 58, 026002 (2018).

[50]M. Jiang, Y. Xu, W. L. Zhong, D. Li, Z. Huang, Z. J. Yang, Z. B. Shi, N. C. Wang, Z. F. Cheng, Z. C. Yang, A. S. Liang, P. W. Shi, J. Wen, Z. Y. Chen, Z. P. Chen, X. M. Pan, P. Shi, B. W. Ruan, D. J. Guo, Q. X. Cai, Q. M. Hu, S. Wang, Y. H. Ding, X. Q. Ji, Y. C. Li, Y. Liu, and M. Xu, Nucl. Fusion 59, 046003 (2019).

[51]M. Jiang, Y. Xu, Z. Shi, W. Zhong, W. Chen, R. Ke, J. Li, X. Ding, J. Cheng, X. Ji, Z. Yang, P. Shi, J. Wen, K. Fang, N. Wu, X. He, A. Liang, Y. Liu, Q. Yang, M. Xu, and HL-2A Team, Plasma Sci. Technol. 22, 080501 (2020).